Nuclear Level-Density Fluctuations and Tests of the Compound Statistical Model*

R. R. JOHNSON† AND NORTON M. HINTZ
School of Physics, University of Minnesota, Minneapolis, Minnesota
(Received 25 April 1966)

Inelastic proton and alpha spectra were observed from (p,p') and (p,α) reactions on Ni^{58}, Ni^{60}, Cu^{63}, Cu^{65}, Zn^{64}, and Zn^{66} at bombarding energies around 10 MeV. Cu^{63} and Zn^{66} inelastic proton yield curves for bombarding energies ranging from 9.5 to 10.5 MeV indicate possible intermediate- or doorway-state resonance structure. Nuclear temperatures T were determined for the residual nuclei in these reactions from plots of $\ln[(d^2\sigma/d\epsilon d\Omega)/\epsilon\sigma_c]$ versus outgoing-channel energy ϵ (where σ_c=inverse cross section), and were found to agree with temperatures from $N(U)$ or Ericson plots (direct level counts) when the temperatures were obtained from nearby excitation regions. Using the level-density formula $\rho(U)=[1/T)\exp[(U-\Delta)/T]$, where U is the residual nuclear excitation, the energy gap Δ was calculated from (p,p')-to-(p,α) yield ratios and found to agree with Δ's obtained from $N(U)$ plots or from Cameron's pairing-energy tables. Departures or fluctuations in the number of levels in an energy interval δU were determined from yield fluctuations and compared with fluctuations predicted from Gaussian probability distributions with variances calculated from several theoretical level-spacing distributions. A Wigner spacing distribution, applicable to nuclear spectra, implies a level-number variance of 0.27 $\bar{N}$, where $\bar{N}+1$ is the average number of levels in an energy interval δU. Analysis of the experimental fluctuations gave a variance of $K\bar{N}$, where $0.1\leq K\leq 0.3$. The method was inverted for high-resolution level-count data to determine T and the energy-gap parameter Δ, which in turn determines the absolute value of the level density. The level-count data showed $K\simeq 0.2$.

I. INTRODUCTION

NUCLEAR reactions at low energy have been compared with great success to the compound-nucleus model first described by Bohr.[1] The application of the model has been most successful in the two limiting regions of single isolated levels (resonance reactions) and of many overlapping levels (compound statistical region). In the compound statistical region, the model has been used to obtain information about nuclear level densities and to predict partial reaction cross sections. A further study of the continuous (unresolved) portion of compound nuclear emission spectra is warranted by recently developed high-resolution experimental techniques. This paper reports the measurement of inelastic proton scattering and (p,α) reactions for medium-weight nuclei at 10-MeV proton bombarding energy. The purpose of the experiment was to obtain information about level densities of the residual nucleus and about fluctuations in level densities, and to make a direct test of the assumptions underlying the compound statistical model. A basic assumption in this analysis is that the reactions proceed by compound nucleus formation and decay as described by the statistical model of nuclear reactions. Ericson[2] and Bodansky[3] have reviewed the theory and only an outline will be given here (Sec. II). Nuclear level densities at $\sim$2-MeV excitation or greater are usually sufficiently large that their average behavior can be given by a continuous function of the excitation energy with two parameters, a nuclear temperature T and an energy gap or pairing energy Δ. One simple function found to fit observed level densities in a number of cases is $\rho(U)=\text{const}\times\exp[(U-\Delta)/T]$, where U is the excitation energy. The compound-statistical theory allows the determination of T from nuclear emission or "evaporation" spectra. More directly, temperatures can also be found from high-resolution spectra where individual levels can be counted to find the average behavior of the level density. A comparison of these two temperatures provides a direct test of the compound statistical assumption, namely, that the decay of the compound nucleus is determined only by barrier-penetration and phase-space factors. One of the authors (NMH)[4] has calculated nuclear temperatures both ways and found moderate agreement.

Many experiments have been done at bombarding energies sufficiently low to expect a large part of the reaction mechanism to be compound-nuclear. For example, Cohen and Rubin,[5] Fox and Albert,[6] and Cindro *et al.*[7] have performed inelastic-proton experiments at $E_p\leq 20$ MeV. Colli *et al.*[8] and Allan[9] have carried out (n,p) studies at $E_n=14$ MeV. Lassen and Sidorov[10] have done (α,p) experiments at 12–20 MeV. Erba, Facchini, and Menchenella[11] have compared nuclear temperatures from spectra studied before 1961. The spectra and angular distributions in these experiments are consistent with a substantial portion of the

* Supported in part by the U. S. Atomic Energy Commission.
† Present address: Nuclear Physics Laboratory, Colorado University, Boulder, Colorado.
[1] N. Bohr, Nature **137**, 344 (1936).
[2] T. Ericson, Advan. Phys. **9**, 425 (1960).
[3] D. Bodansky, Ann. Rev. Nucl. Sci. **12**, 87 (1962).
[4] N. Hintz and V. Meyer, University of Minnesota Linac Progress Report, 59 (1961) (unpublished).
[5] B. Cohen and A. Rubin, Phys. Rev. **113**, 579 (1959).
[6] R. Fox and R. Albert, Phys. Rev. **121**, 587 (1961).
[7] N. Cindro, D. B. Fossan, and D. Zastavniković, Nucl. Phys. **50**, 281 (1964).
[8] L. Colli *et al.*, Nuovo Cimento **13**, 730 (1959).
[9] D. L. Allan, Nucl. Phys. **10**, 348 (1959).
[10] N. O. Lassen and V. Sidorov, Nucl. Phys. **19**, 579 (1960).
[11] E. Erba, U. Facchini, and E. Menchella, Nuovo Cimento **22**, 1237 (1961).

reaction proceeding via the compound-nucleus mechanism. The temperatures calculated are in rough agreement with one another, but with certain discrepancies. Some copper temperatures determined from proton spectra by Meyer and Hintz[4,12] were larger than temperatures determined from neutron spectra by Thomson.[13] Thomson observed a substantial departure from compound-nucleus predictions in low-excitation regions of spectra from medium and heavy nuclei. The departure was attributed to direct inelastic scattering to low-energy states of the residual nucleus.

Most of the previous experiments were done with 2 to 3% resolution and with multichannel analyzers that allowed only a few channels per MeV. Thus only a few data points per MeV were possible. To get enough data points to determine a temperature from the spectra, low-excitation regions were usually included in the analysis, allowing direct reaction scattering to influence the nuclear temperature. Modern solid-state detectors can give $\lesssim 1\%$ resolution, and multichannel analyzers now offer stable channel widths of a few kilovolts so that many data points per MeV can be observed. Good resolution also permits rapid identification of contaminant peaks in the continuum region of the spectra. Therefore, the current experimental techniques offer a means of studying in detail regions where the reaction proceeds almost entirely by the compound-nucleus mechanism.

Nuclear temperatures characterize the average behavior of nuclear-level densities. Since nuclear levels are discrete, there will be fluctuations about the average values of the level density. The study of these fluctuations from high-resolution yield and level-count data will be the principal subject of this paper. Accurate values for nuclear temperatures are important for the analysis and were determined for the nuclei examined in this experiment from the shape of the evaporation spectrum (Sec. IVC). These nuclear temperatures will be compared with those obtained by direct-level counting from high-resolution spectra. Inelastic-proton and alpha cross-section ratios allow the study of pairing energy effects in the level density. A comparison will be made between determinations of the pairing energy parameter, Δ, from high-resolution level counting, odd-even mass differences, and (p,p') to (p,α) yield ratios (Sec. IV D). Sec. V is devoted to examining fluctuations in level distributions from direct level counts.

A summary of the theory and method of analysis is given in Sec. II to provide a background for the presentation of the experimental results (Sec. IV) and conclusions (Sec. VI). A brief description of the experimental methods and data reduction codes is given in Sec. IV.

[12] V. Meyer and N. Hintz, University of Minnesota Linac Progress Report No. 33, 1959 (unpublished).
[13] D. Thomson, Phys. Rev. **129**, 1949 (1963).

II. THEORY

A. Weisskopf-Ewing Formula

Weisskopf and Ewing[14] have described the cross section for a particular emission channel in the compound statistical model by

$$\frac{d\sigma(a,E_b)}{dE_b}=\sigma_c(a)g_b p_b^2\sigma_c(E_b)\rho_b(U_b)\Big/\left(\sum_\nu g_\nu\int_0^\infty p_\nu^2\sigma_c(E_\nu)\rho_\nu(U_\nu)dE_\nu\right), \quad (1)$$

where $\sum_\nu$ is the sum over all open channels, ν a particular channel, p_b the momentum of particle b, $\sigma_c(E_b)$ the inverse cross section for particle b entering the residual nucleus with energy E_b, and $\rho_b(U_b)$ the residual nucleus level density, including the magnetic degeneracy at excitation U_b. $g_b=2S_b+1$, where S_b is the spin of the emitted particle b.

The dynanics of the decay are contained in the inverse cross section, $\sigma_c(E_b)$, while the residual nucleus level density, $\rho(U)$, appears separately in the phase-space portion of (1). By separating the level density of the residual nucleus from the dynamics of the reaction, nuclear models may be studied, comparing level density predictions with experimental data.

B. σ_c Calculation

Using a totally absorbing square-well (continuum) nuclear model with Coulomb wave function, σ_c was calculated with program COMPOUND[15] which is similar to the Shapiro[16] calculation but uses $R=R_0(A_{\text{targ}}^{1/3}+A_{\text{proj}}^{1/3})$. The COMPOUND calculations of σ_c for a proton incident on Cu^{63} are compared with surface-absorption optical-model calculations of σ_c using a code entitled JIB3.[17] The results are shown in Fig. 1. The optical-model parameters for proton energies ranging from 2 to 5 MeV were estimated from the energy dependence of the

TABLE I. Optical-model parameters used in JIB3. $W(SI)$ is the coefficient of surface imaginary potential which is $4(AR)\times W(SI)$ times the derivative of the real Woods-Saxon form factor. RR is the real radius $=RI$, the imaginary potential radius.

E (MeV)	UR (MeV)	$W(SI)$ (MeV)	RR (F)	AR (F)	Reaction cross section (mb)[a]
2.0	49.76	13.5	1.31	0.61	0.662± 0.1
3.0	49.44	12.6	1.31	0.61	32.7± 6.
4.0	49.12	11.8	1.31	0.61	144. ±50.
5.0	48.77	10.85	1.31	0.61	321. ±50.
8.8	...	...	...	...	(776. ±50.)[b]

[a] The error bars for the JIB3 reaction cross sections are estimates of the errors coming from optical-model-parameter uncertainties.
[b] The additional point at 8.8 MeV is an experimental determination of σ_R [P. Bulman, G. Greenlees, and M. Sametbard, Nucl. Phys. **69**, 536 (1965)].

[14] V. F. Weisskopf and D. H. Ewing, Phys. Rev. **57**, 472 (1940).
[15] We are indebted to R. K. Hobbie for the use of his program.
[16] M. Shapiro, Phys. Rev. **90**, 171 (1953).
[17] F. F. Perey, Phys. Rev. **131**, 745 (1963).

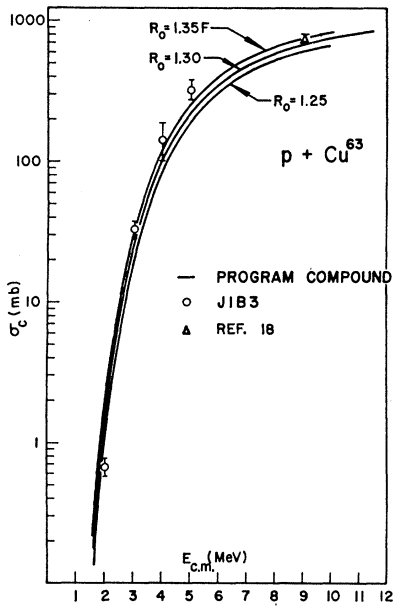

FIG. 1. p+Cu^{63}, logarithm of capture cross section versus $E_{c.m.}$. The error bars on the JIB3 reaction cross sections are estimates of the errors coming from optical-model-parameter uncertainties.

parameters at higher energy. Table I lists the parameters used in JIB3. The validity of such a calculation is doubtful since the optical-model parameters are not well known at low energies. Nevertheless, the calculations should give an idea of the validity of the simple black-nucleus model. The agreement is seen to be good for $R_0=1.35$ F, the black-nucleus radius parameter.

C. Level-Density Functions

The nuclear level density can be described in terms of thermodynamic concepts.[2] An approximation of the level density can be made by expanding the nuclear entropy,

$$S(U)=\ln\rho(U),$$

in a Taylor's series about the excitation $U=0$. When only the first-order term is retained,

$$\rho(U)=\text{const}\times\exp[U/T]=\text{const}\times\exp(-\epsilon/T) \quad (2)$$

where ϵ= channel energy in the outgoing channel.

Assuming the nucleus to be a Fermi gas, the level density can be shown to be[2]

$$\rho(U)\propto(1/U^{5/4})\exp[2(aU)^{1/2}]. \quad (3)$$

Experimental data are frequently analyzed with a simpler level-density formula having the same exponential energy dependence as the preceding equation, namely,

$$\rho(U)=\text{const}\times\exp[2(aU)^{1/2}]. \quad (4)$$

T and a in (2) and (4), respectively, can be found from experiment with the use of (1). T can be found by plotting

$$\ln\left(\frac{d^2\sigma}{d\epsilon d\Omega}\Big/\epsilon\sigma_c\right)\text{ versus }\epsilon,$$

with $-1/T$ being the slope of the line. Plotting

$$\ln\left(\frac{d^2\sigma}{d\epsilon d\Omega}\Big/\epsilon\sigma_c\right)\text{ versus }U^{1/2}$$

will yield a line with slope $2\sqrt{a}$. Equations (2) and (4) tend to fit the experimental data equally well, although some experimenters claim to be able to distinguish between the two forms.[18] The entropy expansion form of the level density, however, agrees more accurately with high-resolution level counting up to excitations about equal to the neutron binding energy.

When angular momentum is included, the level density for all levels,

$$\rho(U)=\textstyle\sum_j\rho(U,j),$$

retains the same energy dependence as (2) or (4). In the analysis to follow we will use the simplest form of the level-density function (2) although values of the parameter a from (4) will be extracted from the data.

D. Ericson Plots

Nuclear temperatures can be found from direct level counts in high-resolution spectra.[18] It is convenient to define

$$N(U)=\int_0^U\rho(E')dE',$$

the total number of states with excitation energy less than U. By plotting $\ln N(U)$ versus the excitation, U, one obtains a staircase function which in many cases can be approximated by a straight line with slope $1/T$ and intercept at $N(U)=1$ of Δ. The equation for the line is thus

$$\ln N(U)=(U-\Delta)/T, \quad (5)$$

where Δ is called the condensation energy and is related to the pairing energy, $P(A)=P(N)+P(Z)$, as defined and tabulated by Cameron.[19] On the average, odd-A nuclei have $\Delta=0$. Δ is negative for odd-odd nuclei and positive for even-even nuclei. For the same A, $|\Delta_{\text{odd-odd}}|+|\Delta_{\text{even-even}}|=P(A)$. Within the errors of the straight-line intercepts determined by the $N(U)$ plot,

$$\Delta_{\text{even-even}}\approx P(A)/2.$$

Fig. 11 shows an $N(U)$ or Ericson plot for Cu^{63}, one of the nuclei investigated in this experiment. In this experiment we will compare nuclear temperatures from evaporation spectra from plots of $(d^2\sigma/d\epsilon d\Omega)/\epsilon\sigma_c$ versus ϵ and from Ericson plots. Δ can also be determined by

[18] T. Ericson, Nucl. Phys. **11**, 481 (1959).
[19] A. G. Cameron, Can. J. Phys. **36**, 1040 (1953).

comparing the inelastic-proton and alpha cross-section ratios as described in the following section.

E. Determination of Δ from Nuclear Spectra Yield Ratios

Rewriting Eq. (5),

$$N(U)=\exp\left[\frac{U-\Delta}{T}\right].$$

But

$$\rho(U)=\frac{d}{dU}N(U)=\frac{1}{T}\exp\left[\frac{U-\Delta}{T}\right],$$

or

$$\rho(U)=\frac{1}{T}\exp\left[\frac{U_M-\epsilon+\Delta}{T}\right],$$

where $U=U_M-\epsilon$. U_M is the maximum possible excitation energy of the residual nucleus, and ϵ the outgoing channel energy.

Since the yield ratios are nearly isotropic, the Weisskopf-Ewing formula can be rewritten,

$$\frac{d^2\sigma(a,\epsilon_\nu)}{d\epsilon_\nu d\Omega}=\left[\frac{\sigma_c(a)2}{4\pi\sum_{\nu'}g_{\nu'}\int_0^\infty p_{\nu'}{}^2\sigma_c(\epsilon)d\epsilon}\right]\times g_\nu m_\nu \epsilon_\nu \sigma_c(\epsilon_\nu)\rho_\nu(U). \quad (6)$$

The cross-section dependence on the Compound nucleus and all decay channels (the bracketed portion) is separated from the factors dependent on the particular decay channel, denoted by ν. Consider the formation of a Compound nucleus and its subsequent decay by way of two different channels, say proton (1) and alpha (2) emission. In this case, the bracketed portion in formula (6) is the same for both emission channels.

Integrating both sides of (6) over $0\leq U\leq U_M$, we obtain,

$$\int_0^{U_M}\frac{d^2\sigma(a,\epsilon_\nu)}{d\epsilon_\nu d\Omega}d\epsilon_\nu=\left[\frac{\sigma_c(a)\times 2}{4\pi\sum_{\nu'}\cdots}\right]g_\nu m_\nu\int_0^{U_{M\nu}}\epsilon_\nu\sigma_c(\epsilon_\nu)\rho_\nu(U)d\epsilon_\nu$$

$$=\left[\frac{\sigma_c(a)\times 2}{4\pi\sum_{\nu'}\cdots}\right]\frac{g_\nu m_\nu}{T_\nu}\int_0^{U_{M\nu}}\epsilon_\nu\sigma_c\exp[-\epsilon_\nu/T]\times\exp\left[\frac{U_{M\nu}-\Delta}{T}\right].$$

We define

$$I_\nu=\int_0^{U_{M\nu}}\frac{d^2\sigma(a,\epsilon_\nu)}{d\epsilon_\nu d\Omega}d\epsilon_\nu,$$

$$f_\nu=\int_0^{U_{M\nu}}\epsilon_\nu\sigma_c(\epsilon_\nu)\exp[-\epsilon_\nu/T]d\epsilon_\nu,$$

and

$$G_\nu=I_\nu/f_\nu,$$

$$G_\nu=\left[\frac{\sigma_c(a)\times 2}{4\pi\sum_{\nu'}\cdots}\right]\frac{g_\nu m_\nu}{T_\nu}\exp\left[\frac{U_M-\Delta}{T_\nu}\right].$$

If we consider emission channels 1 and 2 of the same compound nucleus, then

$$\frac{G_1}{G_2}=\frac{g_1m_1}{g_2m_2}\frac{T_2}{T_1}\frac{\exp[(U_{M1}-\Delta_1)/T_1]}{\exp[(U_{M2}-\Delta_2)/T_2]},$$

or

$$\ln\left[\frac{G_1}{G_2}\frac{g_2m_2}{g_1m_1}\frac{T_1}{T_2}\right]=\left(\frac{U_{M1}-\Delta_1}{T_1}\right)-\left(\frac{U_{M2}-\Delta_2}{T_2}\right). \quad (7)$$

The left side of (7) will be called $\mathfrak{R}$ in the discussion of the experimental results. If one Δ is known, we can determine the other from Eq. (7).

F. Fluctuations in Level Densities

1. Level Fluctuations from Spacing Distributions

Porter and Kahn[20] have described three probability distributions for nuclear and atomic energy-level spacings of a given spin and parity. Letting s be the spacing between adjacent energy levels, the probability distributions can be written

$$p_1(s)=a_1s\exp[-b_1s^2], \quad (8)$$

$$p_2(s)=a_2s^2\exp[-b_2s^2], \quad (9)$$

and

$$p_3(s)=a_3s^4\exp[-b_3s^2]. \quad (10)$$

The distributions are based on the three basic groups of canonical transformations pertaining to quantum systems. The first distribution, Eq. (8), corresponds to the orthogonal group and is called the Wigner distribution. Mehta and Gaudin[22] have shown that $p_1(s)$ is a good approximation of the spacing distribution for nuclear spectra. Systems for which time-reversal invariance is not obeyed follow $p_2(s)$.

When levels of many different spins and parity are considered, the distribution of nearest-neighbor spacings approaches an exponential distribution. Level groups with only a few different spins and parities are expected to have a probability distribution with a shape between an exponential and the Wigner distribution.[22]

The probability distribution for the number of levels η in an energy interval, ΔU, centered at U can, in principle, be obtained for any $p(s)$. The energy interval will be called a bin in following sections of this paper. For $N+1$ levels in an energy bin, $s_1+s_2+\cdots+s_N\leq\Delta U$, where s_i is the spacing between two adjacent levels. Assuming that the spacings are independent, we can define an integral probability,

$$P(\eta)=\text{Probability}\{s_1+s_2+\cdots+s_N\leq\Delta U\},$$

[20] C. Porter and P. Kahn, Nucl. Phys. **48**, 385 (1963).
[21] M. Mehta and M. Gaudin, Nucl. Phys. **18**, 420 (1960).
[22] H. S. Leff, University of Iowa Report, 1963 (unpublished).

which is the probability that the number of levels in ΔU is greater than $\eta=N+1$. Then

$$p(\eta)=\frac{d}{d\eta}P(\eta)=\frac{d}{d\eta}\,\mathrm{Prob}\{s_1+s_2+\cdots+s_{\eta-1}\leq\Delta U\},$$

where $p(\eta)$ is the probability density.

Using the independence assumption and locating the first level at the lower edge of the bin,

$$\mathrm{Prob}\{s_1+s_2+\cdots+s_{\eta-1}\leq\Delta U\}=\int_0^{\Delta U}ds_1p(s_1)$$
$$\times\int_0^{\Delta U-s_1}ds_2p(s_2)\cdots\int_0^{\Delta U-s_1-s_2-\cdots-s_{\eta-2}}ds_{\eta-1}p(s_{\eta-1}).$$

The $(\eta-1)$-fold multiple integral is difficult to evaluate to obtain a closed expression for the η probability distribution. An estimate for the variance of η, $\mathrm{Var}(\eta)$, can be obtained, however, without calculating the $(\eta-1)$-fold integral.

We illustrate with the Wigner distribution, $p(s)=ase^{-bs^2}$. From the normalization of $p(s)$, $a=2b$. The expectation value of s^n, $\langle s^n\rangle$, and the variance of s, $\mathrm{Var}(s)$, can be calculated from $p(s)$ as follows:

$$\langle s^n\rangle=a\int_0^\infty x^{n+1}\exp[-bx^2]dx=\frac{a}{2b^{\frac{1}{2}n+1}}\Gamma(\tfrac{1}{2}n+1).$$

Now defining $\bar{s}\equiv\langle s\rangle$,

$$\bar{s}=\frac{a}{2b^{3/2}}\Gamma(\tfrac{3}{2}),\quad\text{so}\quad b=\frac{\pi}{4\bar{s}^2},$$
$$\langle s^2\rangle=\frac{4}{\pi}\bar{s}^2,$$
$$\mathrm{Var}(s)=\langle s^2\rangle-\bar{s}^2=\left(\frac{4}{\pi}-1\right)\bar{s}^2=0.27\bar{s}^2.$$

For each energy bin ΔU that is examined, a sample average spacing can be found. Let

$$\tilde{s}=(s_1+s_2+\cdots+s_N)/N,$$

where N is the number of spacings in ΔU, and therefore $N=\eta-1$. Aside from an end effect, which we neglect, $\tilde{s}=\Delta U/N$. $\tilde{s}$ is a sample estimate of $\bar{s}$. It has an average $\bar{s}$ and a variance

$$\mathrm{Var}(\tilde{s})=\frac{1}{N}\mathrm{Var}(s)=\frac{0.27}{N}\bar{s}^2. \tag{11}$$

$$\langle\tilde{s}\rangle=\frac{1}{N}\langle s_1+s_2+\cdots+s_N\rangle$$
$$=\frac{1}{N}(\langle s_1\rangle+\cdots+\langle s_N\rangle)=\langle s\rangle,$$

and

$$\mathrm{Var}(\tilde{s})=\mathrm{Var}\left(\frac{1}{N}s_1+\cdots+\frac{1}{N}s_N\right).$$

But if the s are independent,

$$\mathrm{Var}(\tilde{s})=\frac{1}{N^2}\mathrm{Var}(s_1)+\cdots+\frac{1}{N^2}\mathrm{Var}(s_N)=\frac{\mathrm{Var}(s)}{N}.$$

Now $N=\Delta U/\tilde{s}$ and from the calculus of variations,

$$\delta\left(\frac{1}{\tilde{s}}\right)=-\frac{1}{\tilde{s}^2}\delta(\tilde{s}),$$

so

$$\mathrm{Var}(N)=\mathrm{Var}\left(\frac{\Delta U}{\tilde{s}}\right)=\Delta U^2\,\mathrm{Var}\left(\frac{1}{\tilde{s}}\right)=\frac{\Delta U^2}{\bar{s}^4}\mathrm{Var}(\tilde{s})$$
$$=\frac{\Delta U^2}{\bar{s}^2}\frac{(0.27)}{N}. \tag{12}$$

When this analysis is carried out for the other two distributions, (9) and (10), the 0.27 in (12) is changed to 0.18 and 0.10, respectively. An exponential spacing distribution, appropriate to a situation in which levels of different J, π are mixed, would give a coefficient of 1.0.

An approximate form can be found for the distribution of the number of spacings, N, in an energy bin ΔU by assuming that the central-limit theorem of statistics[23] is applicable to describe the distribution of the sample estimate of $\bar{s}$, $\tilde{s}$. As the number of spacings becomes very large, the central limit theorem shows the the distribution of $\tilde{s}$ becomes a Gaussian. Since $\langle\tilde{s}\rangle$ and $\mathrm{Var}(\tilde{s})$ are already known, the distrubtion of $\tilde{s}$ for large N is

$$g(\tilde{s})=\frac{1}{[2\pi\,\mathrm{Var}(\tilde{s})]^{1/2}}\exp\left[\frac{-(\tilde{s}-\bar{s})^2}{2\,\mathrm{Var}(\tilde{s})}\right]. \tag{13}$$

$\bar{s}$ can be written in terms of $\bar{N}$ for some interval, ΔU. Assume m observations of $\tilde{s}$ have been made. Then

$$\langle N\rangle=\Delta U\frac{1}{m}\sum_i\frac{1}{\tilde{s}_i}=\Delta U\frac{1}{m}\sum_i\frac{1}{\bar{s}(1+\delta\tilde{s}_i/\bar{s})},$$

where $\delta\tilde{s}_i$ is the departure of $\tilde{s}_i$ from $\bar{s}$. Taking the first few terms in the expansion of $(1+\delta\tilde{s}/\bar{s})^{-1}$,

$$\langle N\rangle\simeq\frac{\Delta U}{\bar{s}}\left[\frac{1}{m}\sum_i\left(1-\frac{\delta\tilde{s}_i}{\bar{s}}+\frac{1}{2}\frac{(\delta\tilde{s}_i)^2}{\bar{s}^2}\right)\right]$$

or

$$\langle N\rangle\simeq\frac{\Delta U}{\bar{s}}-\frac{\Delta U}{\bar{s}^2}\frac{1}{m}\sum_i\delta\tilde{s}_i+\frac{\Delta U}{2\bar{s}}\frac{1}{\bar{s}^2}\frac{1}{m}\sum_i(\delta\tilde{s}_i)^2.$$

Since $\tilde{s}$ has a Gaussian distribution, $\sum_i\delta\tilde{s}_i=0$ and $(1/m)\sum_i(\delta\tilde{s}_i)^2=\mathrm{Var}(\tilde{s})=0.27\bar{s}^2/N$. The second-order

[23] W. Feller, *Introduction to Probability Theory and its Applications* (John Wiley & Sons, Inc., New York, 1957), 2nd ed., Vol. 1, Chap. 10, p. 229.

term becomes $(\Delta U/2\bar{s})(0.27/N)$, and thus for large N, the average of N becomes

$$\bar{N}\approx\frac{\Delta U}{\bar{s}}\left(1+\frac{0.14}{N}\right)\xrightarrow[\text{large N}]{}\frac{\Delta U}{\bar{s}}. \tag{14}$$

With this approximation, $\mathrm{Var}(N)$ from (12) becomes

$$\mathrm{Var}(N)=(\bar{N}^2/N)(0.27)\simeq\bar{N}(0.27). \tag{15}$$

If levels of different J, π are combined, the variance of the combined numbers distribution will just be equal to the sums of the variances of the individual distributions. Therefore Eq. (15) will still hold for the combined numbers distribution, providing each is a Wigner distribution.

Now $\tilde{s}=\Delta U/N$, so that

$$\mathrm{Prob}(N'\leq N)=1-\mathrm{Prob}(\tilde{s}'\leq\tilde{s}),$$

and

$$\mathrm{Prob}(N'\leq N)=\int_0^N p(N')dN'=1-\int_0^{\Delta U/N} g(\tilde{s}')d\tilde{s}'.$$

But

$$p(N)=\frac{d}{dN}\int_0^N p(N')dN'=\frac{-d}{dN}\int_0^{\Delta U/N} g(\tilde{s}')d\tilde{s}'$$

$$=-g\left(\frac{\Delta U}{N}\right)\frac{d(\Delta U/N)}{dN}$$

so that

$$p(N)=\frac{\Delta U}{[2\pi\,\mathrm{Var}(\tilde{s})]^{1/2}}\frac{1}{N^2}\exp\left\{\frac{-[(\Delta U/N)-\bar{s}]^2}{2\,\mathrm{Var}(\tilde{s})}\right\}.$$

Using (11) and (14),

$$p(N)=\frac{1}{[2\pi(0.27)N]^{1/2}}\frac{\bar{N}}{N}\exp\left[\frac{-(N-\bar{N})^2}{2(0.27)N}\right]. \tag{16}$$

This distribution can be approximated by a Gaussian distribution whose variance is given by (15),

$$p(N)=\frac{1}{[2\pi(0.27)\bar{N}]^{1/2}}\exp\left[\frac{-(N-\bar{N})^2}{2(0.27)\bar{N}}\right]. \tag{17}$$

The result of Eq. (17) could have been obtained directly by invoking the central limit theorem for the numbers distribution. Eq. (17) then applies for the combined numbers distributions for levels of several J, π.

2. *Experimental Data Reduction*

If the T and Δ have been found for a nucleus from the particle emission spectrum and cross-section ratios, or $N(U)$ plots, the percentage departure from $\bar{\eta}$ can be calculated for each energy bin:

$$F=(\eta_{\mathrm{exp}}-\bar{\eta})/\bar{\eta},$$

where F is the fractional departure from $\bar{\eta}$.

The ideal experiment for finding $\mathrm{Var}(\eta)$ is to have M bins with the same $\bar{\eta}$. Then $\mathrm{Var}(\eta)\simeq(1/M)\sum_{\mathrm{bins}}(\eta-\bar{\eta})^2$. This method is impractical. The bins with the same $\bar{\eta}$ that can be obtained from one spectrum are too few to give an accurate value for $\mathrm{Var}(\eta)$, since the nucleus has a level density which increases rapidly with excitation energy.

The most practical way to treat the data is to construct energy bins of equal width and therefore different $\bar{\eta}$, each bin being as small as the experimental resolution will allow. In this way the maximum number of energy bins will be constructed. If T and Δ are known for some nucleus, $\bar{\eta}$ can be computed and hence η using the experimental value of F for each bin. If we assume the probability distribution for η is known, each η and therefore each energy bin has associated with it a cumulative probability, P_t which we can calculate, knowing η and $p(\eta)$:

$$P_t\equiv P(\eta'\leq\eta)=\int_0^\eta p(\eta')d\eta'. \tag{18}$$

P_t is the probability that there will be an η' less than a given η. To show an example, suppose there are M energy bins with equal $\bar{\eta}$. Then for a given cumulative probability $P_t=x$, there will be $x\times M$ bins with cumulative probabilities less than x. Figure 2 shows this relation for $x=1$, $x=0.5$, and $x=0.25$ for a symmetric distribution. Plotting against x the number of bins whose cumulative probability P_t is less than x should result in a straight line, if the correct distribution is assumed.

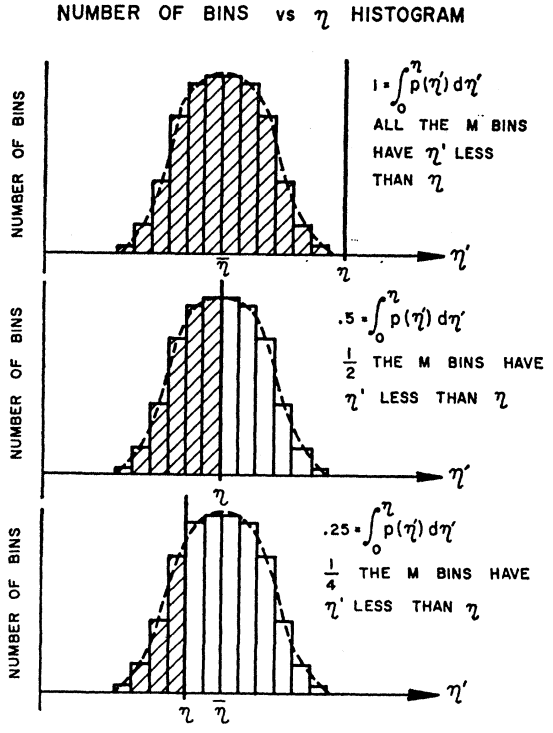

FIG. 2. Histograms of number of bins versus η showing cumulative probability areas for $CP_t=1$, 0.5, and 0.25.

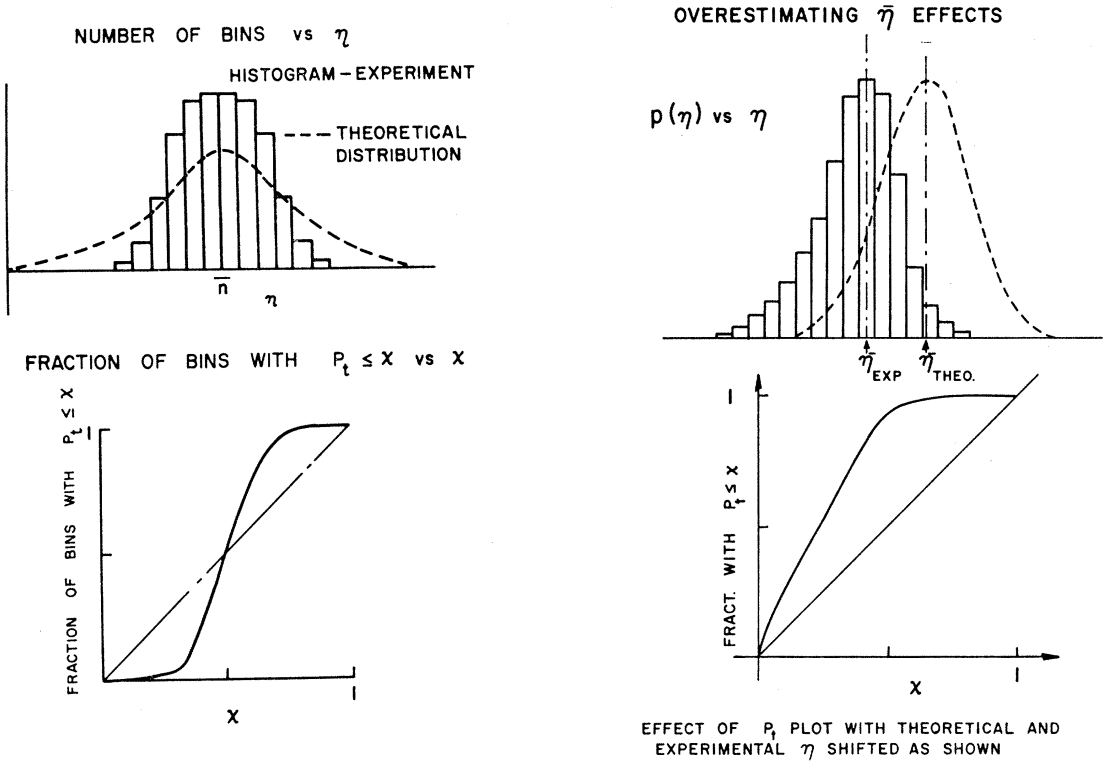

FIG. 3. (a) Histogram of number of bins versus η for experimental data more sharply peaked than the theoretical distribution. (b) P_t plot for case (a), i.e. when the assumed theoretical distribution is too broad. (c) Number of bins versus η for $(\bar{\eta})_{\text{expt}} < (\bar{\eta})_{\text{theor}}$ (d) P_t plot for case (c).

If, however, a bad guess is made for the theoretical distribution, the plot will be nonlinear as shown in Fig. 3. If the assumed $\bar{\eta}$ is correct but a wrong choice is made for $\text{Var}(\eta)$, the curve will be S shaped passing through (0.5,0.5) on the P_t plot. An incorrect $\bar{\eta}$ will result in a curve which does not pass through (0.5,0.5) on the P_t plot.

If the $\bar{\eta}$ dependence of the variance is correct in the assumed distribution, then even when each bin has a different η, a plot of the number of bins with $P_t \leq x$ versus x will be linear.

To learn whether the data follow a given theoretical probability distribution, we must calculate P_t for each bin, count the number of bins with $P_t \leq x$, and plot the resulting numbers versus x. In Sec. IV, the experimental data will be compared with a Gaussian distribution centered at $\bar{\eta}$ with $\text{Var}(\eta)=0.27(\bar{\eta}-1)$ [appropriate for a Wigner distribution, Eq. (8)] and $\text{Var}(\eta)=0.1(\bar{\eta}-1)$ [distribution of Eq. (10)]. In Sec. V P_t plots will be presented for direct level counts from high-resolution spectra.

III. EXPERIMENTAL APPARATUS AND RAW DATA

A. Experimental Apparatus

Ten MeV is an ideal energy for these experiments since it is low enough for the bulk of the reaction to proceed by a compound nucleus and it is below the two-particle emission threshold for all practical purposes. Yet 10 MeV is sufficiently above the Coulomb barrier for medium-A nuclei to give moderately large inelastic and reaction cross sections.

To obtain accurate temperatures and reaction-cross-section ratios and to see yield fluctuations due to fluctuations in the number of levels in an energy bin, a good-resolution, low-background, and stable-charged-particle detection system was developed for the Minnesota linear accelerator proton beam at the 10-MeV exit port. The system is fairly conventional, so only an outline of its characteristics is given here. Further details are available in unpublished laboratory reports.[24,25]

The system consisted of a solid-state detector within a 24-in. scattering chamber,[26] a Goulding preamplifier,[27,28] a Tennelec TC200 postamplifier, and a Nuclear Data 150FM pulse-height analyzer (PHA) with an associated beam-gating chassis. Figure 4 shows the over-

[24] J. Durisch and R. Johnson, University of Minnesota Linac Progress Report No. 87, 1963 (unpublished).
[25] R. Johnson and N. Hintz, University of Minnesota Linac Progress Report No. 36, 1964 (unpublished).
[26] N. Hintz, Phys. Rev. **106**, 1201 (1957).
[27] F. S. Goulding and D. Landis, Natl. Acad. Sci.—Natl. Res. Council, Publ. **1184**, 61 (1964).
[28] G. Nelson, University of Minnesota Linac Progress Report, 1965 (unpublished).

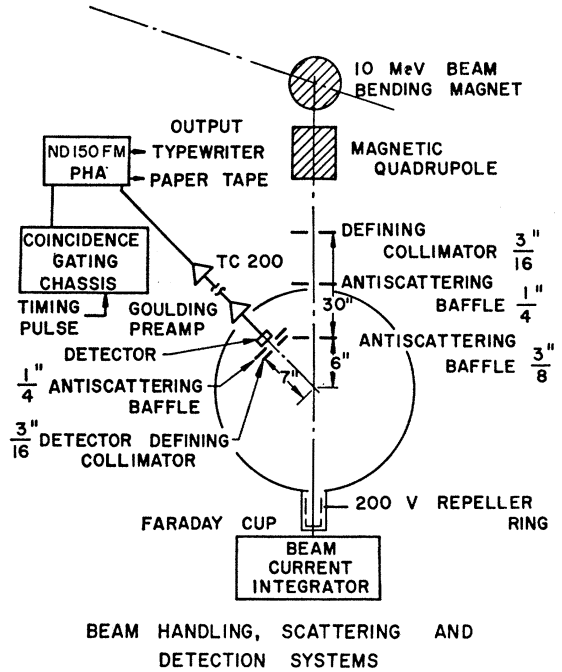

FIG. 4. Beam handling, scattering, and detection systems for data taken at the University of Minnesota linear accelerator. Data were taken at the Argonne tandem Van de Graaff accelerator with similar apparatus.

all beam-handling system, the detector, and the pulse-height-analyzer system.

The resolution (full width at half-maximum, FWHM) of the proton detection system, tested with 8.78- and 6.05-MeV alpha particles from a Po^{212} source, was 40 keV; tested with 10-MeV protons elastically scattered from Gold it was 60 keV. During production experimental runs of 4 to 36 h, the FWHM ranged from 80 to 100 keV depending on accelerator stability and tuning. Table II gives a breakdown of the experimental resolution.

B. Targets and Detectors

Medium-A nuclei ($A=58$ to $A=66$) were chosen for several reasons. Much experimental work has been done in this region and the level densities are large enough at low excitation for a statistical description to be applicable. Targets relatively free from contaminants were available. Even- and odd-A nuclei were chosen to observe pairing-energy effects in the level densities.

TABLE II. Contributions to experimental resolution for typical runs.

Component	Resolution (keV)
Detector noise	25
Preamplifier noise	25
PHA bins	20
Beam energy spread and stability	80
Total resolution	90

Angular distributions of proton and alpha spectra were taken on Zn^{66}, Cu^{63}, Cu^{65}, and Ni^{58} targets using the 9.89-MeV proton beam of the University of Minnesota linear accelerator. Proton spectra at a scattering angle of 135° were also taken on Zn^{64} and Ni^{60} targets, as well as an alpha spectrum of the Zn^{64} target. The experimental uncertainty in the angle was $\pm 0.1°$. Relative percentage errors in the total inelastic proton yields ranging from $\pm 1\%$ to $\pm 2\%$ at forward angles are due to uncertainties in the subtraction of elastic protons and contaminant yields. At 135° the uncertainty in the inelastic proton yield is only 0.5% and is mostly due to errors in subtracting contaminant contributions to the spectra. Protons from the Argonne tandem Van de Graaff accelerator were used to study inelastic proton and alpha spectra in 100-keV steps from 9.5 to 10.5 MeV from Cu^{63} to Zn^{66} targets. The target thicknesses and enrichments are given in Table III.

Proton-plus-alpha spectra were taken with a Nuclear Diodes surface-barrier silicon detector (depletion depth $\sim 750\,\mu$) and with a TMC lithium-drifted detector (depletion depth $\sim 1000\,\mu$). Alpha spectra were taken by replacing the thick stopping detector by a thinner detector, a surface barrier detector with a depletion depth of $\sim 130\,\mu$, which was used as a proton passing detector. A 10-MeV proton deposited only 4 MeV in the thin detector, which could stop up to 17-MeV alpha particles. Figure 5(a) shows an example of a proton-plus-alpha and an alpha spectrum. Figure 5(b) shows the subtracted spectrum for the inelastic protons alone. Deuteron contamination of the spectra is not possible since (p,d) reactions with these targets have large negative Q values. As a result, the deuteron laboratory energies fall below the energies investigated in the experiment. For example, the $Cu^{63}(p,d)Cu^{62}$ reaction has $Q=8.57$ MeV, leading to a maximum deuteron energy at the detector of 0.89 MeV at an angle of $\theta=135°$.

C. Data Reduction

Calculation of nuclear temperatures and the fluctuations of η require that the same numerical operations be performed on nearly all channels of a pulse-height-analyzer spectrum. For example, to calculate T, $\ln[(d^2\sigma/dEd\Omega)/\sigma_c]$ must be calculated for each energy bin for energies corresponding to the continuum spec-

TABLE III. Average target thicknesses.

Target	Enrichment	Average thickness (mg/cm²)
$_{30}Ni_{28}^{58}$	99.5	0.9295±0.0005[a]
$_{30}Ni_{28}^{60}$	99.8	1.0193±0.0006
$_{34}Zn_{30}^{64}$	99.85	0.9602±0.0005
$_{36}Zn_{30}^{66}$	98.8	0.9626±0.0005
$_{36}Cu_{29}^{65}$	99.7	0.9839±0.0005
$_{34}Cu_{29}^{63}$	99.9	1.079 ±0.0007

[a] The errors in the average thicknesses are smaller than the thickness errors due to target nonuniformity.

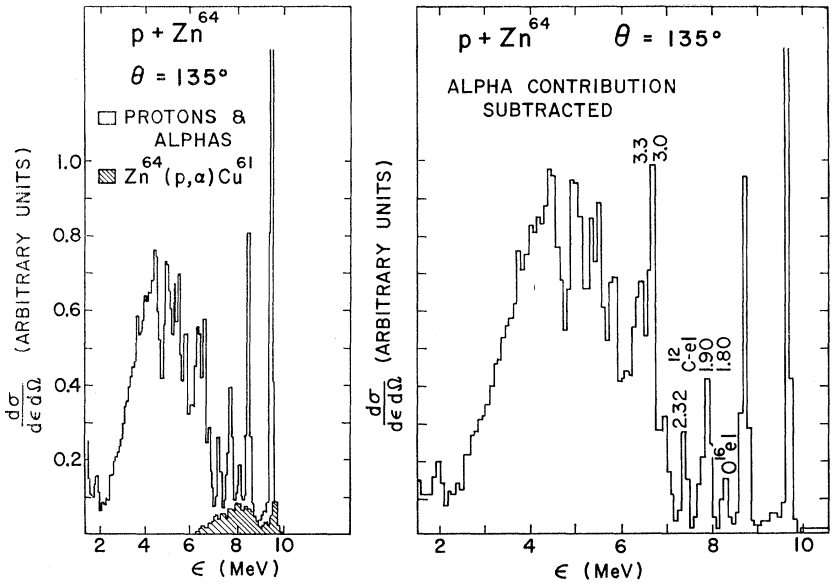

FIG. 5. (a) $Zn^{64}(p,p')Zn^{64}$ and $Zn^{64}(p,\alpha)Cu^{61}$ spectra versus channel energy showing the relative positions of proton and alpha contributions to the pulse-height spectra. (b) Resultant spectrum when alpha contribution is subtracted. Excitation energies shown on the figure were calculated in CNNUCI (see Fig. 6).

trum of the residual nucleus. The outgoing reaction channel energy ϵ must be calculated for each channel of the pulse-height analyzer. These calculations and others outlined in Sec. II were programmed for the University of Minnesota CDC 1604 computer.

The PHA spectra were recorded on paper tape. After the experimental runs, the tape was used to punch cards on an IBM 47 tape to card reader. The card data were then analyzed on the CDC 1604 computer using the Numerical Analysis Center's Fortran 60 Monitor System, a FORTRAN language system that is similar to FORTRAN IV, but also allows use of machine symbolic instructions and pseudo-instructions. Figure 6 is a schematic outline of the programs that were used to calculate channel energies, cross sections, nuclear temperatures, Δ's, and to examine fluctuations in η. The basic energy calibration for protons was determined by calculating the laboratory energy of the elastic peak and then finding the pulse-height-analyzer channel energies from the linearity of the detection system. Alpha spectra energies were calibrated from spectra taken of a Po^{212} source. Good agreement between published and experimental excitation energies and reaction Q values was obtained. Table IV shows a comparison of published and experimental values of excitation energies as well as predicted and observed laboratory energies of some contaminant peaks calculated with computer code CNNUCI. Table V compares some published and experimental (p,α) Q values calculated with computer code ALPHA.

IV. EXPERIMENTAL RESULTS

A. Angular Distributions

Since spectra were observed at only a few angles, generally 65°, 90°, 115°, and 135°, only a qualitative comparison of the experimental angular distributions with compound-statistical theory will be made. Using Ericson's semiclassical formula[29] and the rigid-body moment of inertia to calculate the spin-cutoff parameter, σ, the angular distribution for Cu^{63} is

$$(\sigma(\theta)/\sigma(\tfrac{1}{2}\pi)) \approx 1+\tfrac{1}{2}\xi\cos^2\theta = 1+0.14\cos^2\theta,$$

where $\xi=\bar{I}^2\bar{l}^2/(2\sigma^2)^2$, σ is the spin-cutoff parameter, $\bar{I}$ is

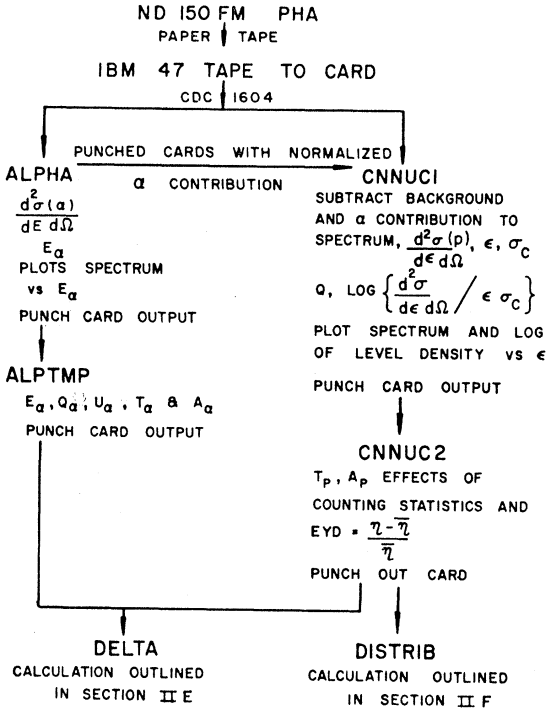

FIG. 6. Outline of data-reduction programs. The computer calculations were broken into short programs so that errors could be easily corrected.

[29] T. Ericson and V. Strutinski, Nucl. Phys. 8, 284; 9, 689 (1959).

TABLE IV. Comparison of published energies with experimental energies in MeV for target and contaminant peaks.[a]

Target	Published excitation energy (MeV)[b]	Experimental excitation energy (MeV)	Calculated[a] detector energy (MeV)	Experimental[a] detector energy (MeV)
Cu^{63}	0.668	0.675±0.010	...	...
Cu^{63}	0.961	0.970±0.010	...	...
Cu^{63}	1.547	1.558±0.020	...	...
	C^{12} elastic contaminant (E_p=9.89)		7.37	7.36±0.02
	C^{12} 4.43-MeV state		3.59	3.50±0.04
Cu^{65}	0.770	0.76±0.01	...	...
Cu^{65}	1.482	1.49±0.01	...	...
Cu^{65}	1.725	1.73±0.01	...	...
	C^{12}, elastic contaminant (E_p=9.89)		7.35	7.39±0.01
	C^{12} 4.43-MeV state		3.55	3.56±0.01
	O^{16}, second 2^+ state		1.76	1.76±0.04
Zn^{64}	0.99	1.00±0.02	...	...
Zn^{64}	1.78	1.80±0.02	...	...
Zn^{64}	2.29	2.31±0.02	...	...
Zn^{64}	3.0	3.04±0.02	...	...
Zn^{64}	3.3	3.36±0.02	...	...
Zn^{66}	1.037	1.037±0.010	...	...
Zn^{66}	1.865	1.896±0.02	(obscured by C^{12} elastic peak)	
Zn^{66}	2.37	2.38 ±0.01	...	...
Zn^{66}	2.76	2.81 ±0.01	...	...
	O^{16}, contaminant, second-2^+ state (E_p=10.0)		1.87	1.90±0.04
	O^{16}, first 3^- state		2.58	2.56±0.03

[a] Energies at the detector for contaminant peaks are compared with calculated values for a scattering angle of 135°.
[b] Excitation energies were taken from H. H. Landolt and R. Börnstein, *Energy Levels of Nuclei A=5 to A=257* (Springer-Verlag, Berlin, 1961), Vol. 7.

the average angular momentum of the residual nucleus, and $\bar{l}$ is the average angular momentum of the emitted particle.

Using this analysis, one would expect similar angular distributions for Ni^{58}, Cu^{65}, and Zn^{66} since the radii are nearly the same and hence $\bar{I}$, $\bar{l}$, and σ. Figure 7 shows

TABLE V. Comparison of calculated and experimental (p,α) Q values for some spectra analyzed with code ALPHA.

Reaction	Residual excitation energy[a] (MeV)	(p,α) Q value (calc.)[b] (MeV)	(p,α) Q value (expt.) (MeV)
$Cu^{63}(p,\alpha)Ni^{60}$	0	3.776	(Off PHA scale)
	1.332	2.444	2.45±0.01
	2.159	1.617	1.62±0.01
$Cu^{65}(p,\alpha)Ni^{62}$	0	4.344	(Off PHA scale)
	1.72	3.172	3.17±0.01
	2.303	2.041	not resolved
	2.336	2.008	not resolved
	3.25	1.09	1.09±0.01
$Zn^{64}(p,\alpha)Cu^{61}$	0	0.8290	0.83±0.01

[a] Excitation energies were taken from H. H. Landolt and R. Börnstein, *Energy Levels of Nuclei A=5 to A=257* (Springer Verlag, Berlin, 1961), Vol. I.
[b] Ground-state Q values were taken from V. J. Ashby and K. C. Catron, University of California Radiation Laboratory Report No. 5419, 1959 (unpublished).

the angular distributions of integrated proton yields over two regions of excitation compared with isotropic distributions. The errors are within the width of the data points. For the range of angles observed, $\sigma(\theta)/\sigma(\pi/2)$ has about a 7% change. Some of the angular distributions show a small departure from isotropy, but the data is not sufficiently accurate to obtain a value of the spin cutoff parameter. The departures from isotropy tend to be greater when low-excitation regions are included (i.e., ϵ=6–8 MeV). This effect could be due to the energy dependence of the spin cutoff parameter σ given by Gilbert and Cameron,[30] $\sigma^2 \propto U^{1/2}$, so that particles emitted to regions of low excitation should exhibit a greater anisotropy than those emitted to higher-excitation regions.

B. Proton and Alpha Yields Versus Bombarding Energy

Two types of fluctuations or resonances might be expected in the yield versus bombarding energy to a given final state or group of states: compound nuclear or Ericson,[31] and intermediate resonance or doorway state.[32] If there are groups of residual nuclear states preferentially excited at certain compound nucleus energies, the temperatures obtained from evaporation spectra could vary with bombarding energy. These characteristics are discussed in Sec. IVC. To study possible intermediate resonance structure, Cu^{63} and Zn^{66} targets were bombarded with 9.5 to 10.5 MeV protons at the Argonne tandem Van de Graaff accelerator.

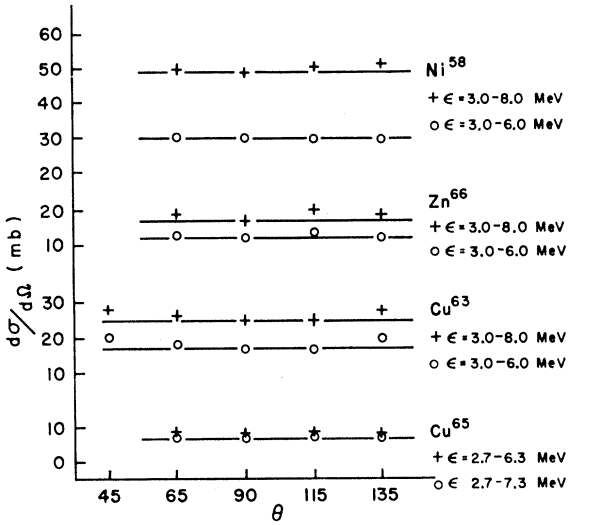

FIG. 7. Inelastic proton angular distributions for selected excitation regions as indicated for Ni^{58}, Zn^{66}, Cu^{63}, and Cu^{65}. Errors are within the widths of the data points.

[30] A. Gilbert and A. G. Cameron, National Aeronautics and Space Administration Goddard Space Flight Center Report, 1965 (unpublished).
[31] T. Ericson, Ann. Phys. (N. Y.) 23, 439 (1963).
[32] A. K. Kerman, L. S. Rodberg, and J. E. Young, Phys. Rev. Letters 11, 422 (1963).

Proton-plus-alpha and alpha spectra were taken at 135° with a detection system similar to that used at Minnesota and described in Sec. IIIA. The compound nucleus excitation width of about 50 keV was due to beam resolution and energy loss in the target.

Though the bombarding energy was varied in rather large increments (100 keV), some structure is visible in the yield curves. Figures 8 and 9 are proton yield curves for Zn^{66} and Cu^{63}, respectively. In these figures, the errors are indicated by the widths of the data points unless error bars are shown. Compound nuclear (Ericson) fluctuations of the yields to different residual nuclear states should not be correlated, while intermediate-state resonances to different states should be correlated. The discrete state yield curves in Figs. 8 and 9 appear to be correlated at some energies and not at others. The yield curves for portions of the continuum region seem to have a greater correlation and hence suggest the presence of intermediate resonances since the Ericson fluctuations would decrease as the number of final states is increased. The data, however, is not sufficiently extensive for a determination of the resonance parameters.

C. Nuclear Temperatures and $N(U)$ Plots

Nuclear temperatures were calculated from $\ln \times[(d^2\sigma/dEd\Omega)/\epsilon\sigma_c]$ plots for inelastic proton and alpha spectra, finding the slope by the method of least squares[33] each point being weighted equally. These calculations were done with program CNNUC2 described in Sec. IIIC. An inelastic-proton temperature plot is shown in Fig. 10 for Zn^{64}.

Calculations of σ_c from the continuum model[16] for different R_0 gave curves with about the same slope but different normalizations. Cu^{63} inelastic proton tempera-

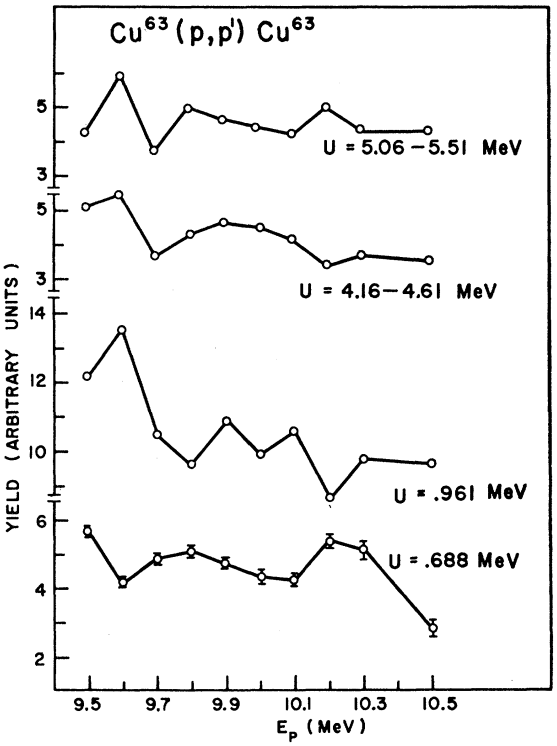

FIG. 9. Cu^{63} proton yields for bombarding energies ranging from 9.5 to 10.5 MeV at 135° for excitation energies shown. Errors are within the circles unless otherwise shown.

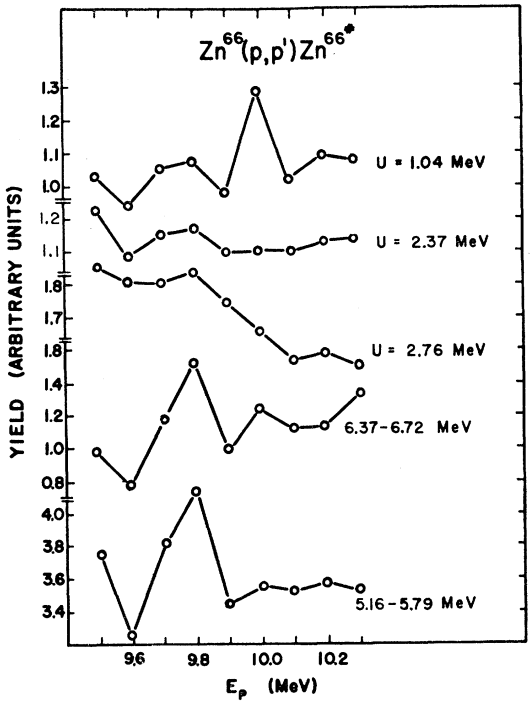

FIG. 8. Zn^{66} proton yields for bombarding energies ranging from 9.5 to 10.3 MeV at 135° for excitation energies shown. Errors are within the widths of the circles.

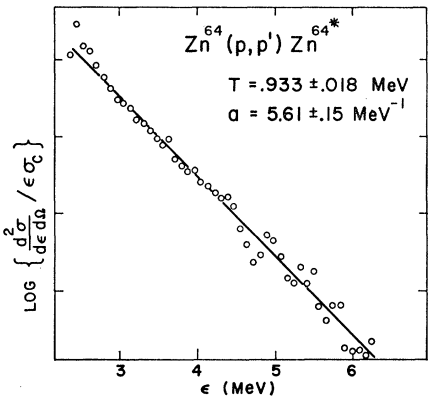

FIG. 10. Spectrum temperature plot for Zn^{64} inelastic protons, $\ln[(d^2\sigma/d\epsilon d\Omega)/\epsilon\sigma c]$ versus channel energy ϵ; $R_0 = 1.30$ F. Counting statistics are within widths of points.

[33] E. L. Grow, F. A. Davis, and M. W. Maxfield, *Statistics Manual* (Dover Publications, Inc., New York, 1960).

TABLE VI. Nuclear temperatures and Fermi-gas a's [Eq. (4)] for Cu^{63} determined from proton-spectrum data for excitation interval $U=3.6$ to 7.4 MeV.

R_0 (F)	T (MeV)	a (MeV^{-1})	Alpha subtraction
1.25	0.942±0.008	6.04±0.06	Yes
1.30	0.968±0.008	5.72±0.06	Yes
1.35	0.995±0.008	5.41±0.06	Yes
1.30	0.978±0.008	5.59±0.06	No

tures were calculated for $R_0=1.25$, 1.30, and 1.35 fermis. Table VI gives the results of these calculations together with one calculation in which the alpha contribution was not subtracted from the charged particle spectrum. The error assignment is the calculated standard error[33] from the least squares fit for Tables VI and VII.

Table VII shows inelastic-proton and alpha temperatures for $R_0=1.30$ fermis obtained from runs at the Minnesota linear accelerator, as well as temperatures found from the corresponding $N(U)$ plots. The inelastic-proton and alpha temperatures were calculated for the excitation regions shown in the table. The excitation regions were chosen to coincide with straight-line portions of the temperature plots and to avoid the lowest states.

For odd-A nuclei, temperatures from $N(U)$ plots were found from lines constrained to pass through $\Delta=0$ (see Sec. II D) and through the higher excitation regions. The temperatures from the $N(U)$ plots generally agree with those from the inelastic proton spectra, although in general only the lower excitation range of the evaporation plots overlapped with the range of the $N(U)$ plot. Even-A nuclei do not have $\Delta=0$ so the $\Delta=0$ constraint could not be used. The Cu^{63} and Ni^{60} temperatures determined from alpha spectra are smaller than those obtained from proton spectra, but agree with $N(U)$ temperatures when low-excitation regions of the $N(U)$ plots are used and the $\Delta=0$ constraint is dropped. Temperatures agree, in other words, when the straight line is drawn through regions of excitation of the $N(U)$ plots corresponding as nearly as possible to those excitation regions used to determine the spectrum temperature. An example of an $N(U)$ plot for Cu^{63} is shown in Fig. 11.

When the excitation interval in the evaporation spectra was increased to include lower states of the residual nucleus, the resultant temperatures increased. The largest increase was for Cu^{65}, where the temperature for excitation interval 2.8 to 6.9 MeV was 1.09 MeV, and that for 1.1 to 6.9 MeV was 1.29 MeV, an increase in the nuclear temperature of about 20%. This increase can be attributed to the direct reaction component of the yield which is concentrated mainly at the lower excitation regions of the residual nucleus.[13]

Alpha and proton temperatures were calculated for the $Zn^{66}(p,p')Zn^{66}$ and $Zn^{66}(p,\alpha)$ spectra taken in 100 keV steps at the Argonne tandem for an alpha excitation region of 2.0 to 4.8 MeV and a proton-excitation region of 3.0 to 6.0 MeV for the residual nucleus. The alpha results are shown in Fig. 12, the proton results in Table VIII. The average proton temperature for the Argonne experiment is $T=0.90$ MeV, compared to the $N(U)$ temperature of 0.85±0.1 MeV. Both proton and alpha temperatures show a small rise with increasing bombarding energy. It is not known why the Argonne proton and alpha temperatures are slightly lower than the Minnesota temperatures. The differences could be due to slightly different background and contaminant conditions.

The ±7 percent variation over the bombarding energy interval in Fig. 12 and Table VIII shows the limitation on the accuracy of temperatures obtained from evaporation spectrum using the compound-statistical theory in its simplest form in which angular-momentum effects are neglected. However, the evaporation temperature values are still within the errors of those from $N(U)$ plots. When the proton and alpha yield ratios are used to determine Δ (Sec. IV D), the accuracy in Δ will be determined by the standard error of T rather than by the over-all uncertainty in T, since in this case T has

TABLE VII. Temperature comparison for nuclei studied in this experiment for $R_0=1.30$ F and $R=R_0(A_{\text{targ}}^{1/3}+A_{\text{proj}}^{1/3})$, $\theta=135°$, $E_p=9.89$ MeV.

Residual nucleus	Reaction	Excitation region (MeV)	T (MeV) spectra	a (MeV^{-1}) spectra	T (MeV) $N(U)$ plots[a]	Maximum U in $N(U)$ plots (MeV)
Ni^{58}	$Ni^{58}(p,p')$	5.6–7.2	0.92 ±0.02	7.5±0.2	0.84 ±0.08	3.0
Ni^{60}	$Ni^{60}(p,p')$	4.1–7.6	0.92 ±0.03	7.1±0.3	0.89 ±0.09	3.1
Ni^{60}	$Cu^{63}(p,\alpha)$	2.3–7.1	0.73 ±0.01	8.5±0.8	0.74 ±0.07	3.1
Cu^{61}	$Zn^{64}(p,\alpha)$	1.0–4.1	0.62 ±0.01	5.8±0.6	···	
Ni^{62}	$Cu^{65}(p,\alpha)$	2.6–7.5	0.76 ±0.01	8.2±0.8	0.76 ±0.08	3.5
Cu^{63}	$Cu^{63}(p,p')$	3.6–7.4	0.968±0.008	5.7±0.2	0.914±0.05	3.2
Cu^{63}	$Zn^{66}(p,\alpha)$	2.0–5.3	0.62 ±0.01	8.9±0.4	0.72 ±0.04	2.7
Cu^{65}	$Cu^{65}(p,p')$	2.8–6.9	1.09 ±0.01	3.8±0.3	1.0 ±0.1	3.0
Cu^{65}	$Cu^{65}(p,p')$	1.1–6.9	1.29 ±0.02	2.0±0.3	1.0 ±0.1	3.0
Zn^{64}	$Zn^{64}(p,p')$	2.9–7.5	0.933±0.018	5.6±0.6	1.1 ±0.1	3.3
Zn^{66}	$Zn^{66}(p,p')$	2.8–6.4	0.99 ±0.01	4.7±0.4	0.85 ±0.1	4.8

[a] $N(U)$ temperatures were obtained by weighting most heavily the energies closest to excitation regions used in determining the appropriate spectrum temperatures. The fits to the $N(U)$ plots were made by eye (See however Table XI). Estimates of the errors involved in this procedure are given in the table. The data for the $N(U)$ plots is from H. H. Landolt and R. Burstein (Ref. a, Table V) and *Nuclear Data Sheets*, compiled by K. Way *et al.* (Printing and Publishing Office, National Academy of Sciences—National Research Council, Washington 25, D. C.).

TABLE VIII. T and a dependence for Zn^{66} on bombarding energy for excitation interval of 3.0 to 6.0 MeV, $\theta=135°$.

E_p (MeV)	$T(\pm 2\%)$ (MeV)	$a(\pm 4\%)$ (MeV^{-1})
9.5	0.84	6.7
9.6	0.89	6.0
9.7	0.86	6.6
9.8	0.84	6.9
9.9	0.92	5.7
10.0	0.92	5.7
10.1	0.92	5.7
10.2	0.96	5.3
10.3	0.96	5.2

been determined to give the best fit to a particular spectrum at a given bombarding energy. The standard error, as discussed above, is an estimate of the error in T from the least-squares fit to the data points.

The changes in T from the alpha spectra are mainly due to fluctuations in the first few excited state yields.

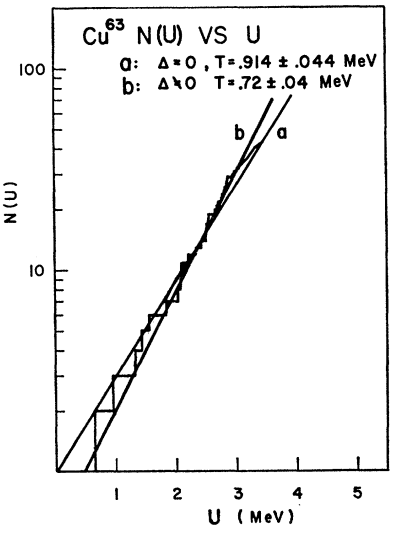

FIG. 11. Cu^{63} total number of levels, $N(U)$ up to excitation energy U versus U. When Δ is constrained to be zero and more weight is given to higher excitation regions, a nuclear temperature is found that agrees with inelastic proton spectrum temperatures.

The ground-state yield curve is also shown in Fig. 12 to compare with the energy dependence of the temperature.

D. EXPERIMENTAL Δ

Program DELTA was used to calculate $\mathfrak{R}$, defined in Eq. (7), to find Δ for the even-even residual nuclei Ni^{60}, Ni^{62}, Zn^{64}, and Zn^{66}, using $\Delta=0$ for the odd-A

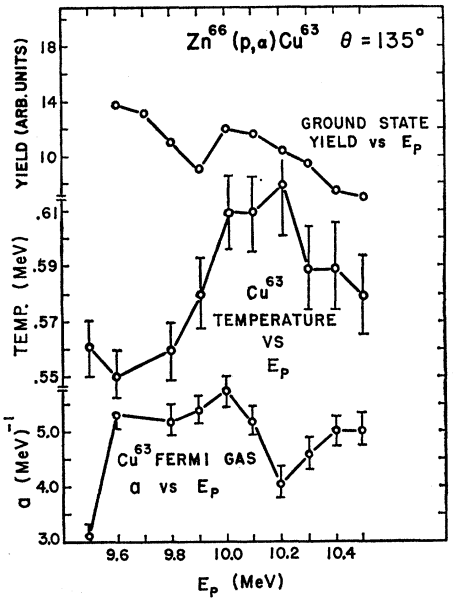

FIG. 12. Ground-state yield curve, temperatures, and a values for $Zn^{66}(p,\alpha)Cu^{63}$. Errors are within the circles unless otherwise shown.

nuclei. The resultant values are compared with Δ obtained from $N(U)$ plots and from Cameron's pairing energy values[19] in Table IX.

The R_0 dependence of σ_c (Fig. 1) has only a small effect on Δ. To illustrate, proton Cu^{63} temperatures were calculated for $R_0=1.25$, 1.30, and 1.35 (Table VI). With these temperatures and the corresponding σ_c's, Δ was calculated. Table X shows the dependence of Δ on R_0 is small. Changing R_0 and T tends to change only the normalization but not the shape of the predicted yield curves. However, the yield ratios are only slightly affected. The error in Δ is mainly due to errors in T_p and T_α. For δT_p and δT_α independent,

$$(\delta\Delta_\alpha)^2=(\mathfrak{R}-U_{M_p}/T_p)^2(\delta T_\alpha)^2+(U_{M_p}T_\alpha/T_p^2)^2(\delta T_p)^2,$$

when $\Delta_p=0$ (odd inelastic proton residual nucleus), and

$$(\delta\Delta_p)^2=(\mathfrak{R}+U_{M_p}/T)^2(\delta T_\alpha)^2+(U_{M\alpha}T_p/T_\alpha^2)^2(\delta T_\alpha)^2,$$

when $\Delta_\alpha=0$ [odd (p,α) residual nucleus]. The last term in the second equation can give a large error for Δ_p since $T_p>T_\alpha$. This effect does not appear in the first

TABLE IX. Δ values determined from yield ratios[a] and $N(U)$ plots compared with Cameron's pairing energy values.

Yield ratio	Nucleus	Δ (MeV) Experiment	Δ (MeV) $N(U)$	Cameron[b] $[P(N)+P(Z)]/2$
$Cu^{63}(p,p')Cu^{63}/Cu^{63}(p,\alpha)Ni^{60}$	Ni^{60}	1.46±0.17	1.4+0.2	1.42
$Cu^{65}(p,p')Cu^{65}/Cu^{65}(p,\alpha)Ni^{62}$	Ni^{62}	1.30±0.16	1.4±0.2	1.40
$Zn^{64}(p,p')Zn^{64}/Zn^{64}(p,\alpha)Cu^{61}$	Zn^{64}	1.35±0.26	1.0±0.2	1.27
$Zn^{66}(p,p')Zn^{66}/Zn^{66}(p,\alpha)Cu^{63}$	Zn^{66}	1.31±0.31	1.0±0.2	1.28

[a] Δ assumed equal to zero for the odd-A residual nucleus.
[b] Reference 19.

TABLE X. R_0 dependence of Δ for Ni^{60} from $Cu^{63}(p,p')Cu^{63}/Cu^{63}(p,\alpha)Ni^{60}$ yield ratio.

R_0 (F)	Δ (MeV)
1.25	1.47
1.30	1.46
1.35	1.46

equation, and thus Δ_α gives the most reliable estimate of Δ.

E. FLUCTUATIONS

Departures from the smooth inelastic yield spectra predicted by continuous level density formulas were analyzed with the techniques described in Sec. IIF. The percentage departures of the number of levels from the average

$$F(\epsilon)=(\eta_{\text{exp}}-\bar{\eta})/\bar{\eta}$$

were calculated in CNNUC2 and, together with the temperature and Δ, were run in program DISTRIB to check the consistency of $F(\epsilon)$ with a Gaussian distribution having mean $\bar{\eta}(\epsilon)$ and a variance $K(\bar{\eta}-1)$, where $0.1\leq K\leq 0.3$. For the calculation of $\bar{\eta}$, spectrum T's and yield ratio Δ's were used. The approximate Gaussian distribution, Eq. (17) derived from a Wigner spacing distribution, has a simpler form than the more exact Eq. (16) and so was used in the analyses. Figure 13, which contrasts the two distributions for $\bar{\eta}=50$, shows that the more exact distribution is skewed slightly, but not enough to be experimentally distinguished from the gaussian distribution.

Both experimental resolution and counting statistics will tend to damp the fluctuations about $\bar{\eta}$. Experimentally, fluctuations due to counting must be made smaller than the variations expected from level number fluctuations. $F(\epsilon)$ was found to vary roughly from 0 to $\pm 10\%$ for the largest bin size, so counting statistics were chosen to give, at most, a 2% error in the yield of each bin. This corresponded to 2.5×10^3 counts per bin and therefore required long runs. The counting-statistics effects were examined qualitatively in CNNUC2 by making a mock temperature plot where all the departures were due to randomly distributed counting-statistics errors. An experimental Cu^{63} inelastic-proton temperature plot is shown in Fig. 14 together with the counting statistics simulation of the same plot. The figure shows that the counting-statistics fluctuations account for only a small portion of the departures for this run.

To compare the fluctuations with the results expected for a Gaussian distribution, $\bar{\eta}$ was calculated from T and Δ. The experimental F was used to calculate η, and then to find P_t for each bin. The number of bins with $P_t\leq x$ was counted for $0\leq x\leq 1$ and plotted against x. The results for various cases are shown in Figs. 15 and 16. P_t plots were not made for Cu^{65} because of inadequate counting statistics, or for Ni^{58} and Ni^{60} because the level densities were too low. $\bar{\eta}$ for the bins studied in this experiment ranged from $\bar{\eta}=3$ for the lowest excitation region to $\bar{\eta}=50$ for the highest. The number of bins was typically 40–60.

Poor resolution may damp the fluctuations in η when the experimental energy resolution R is much larger

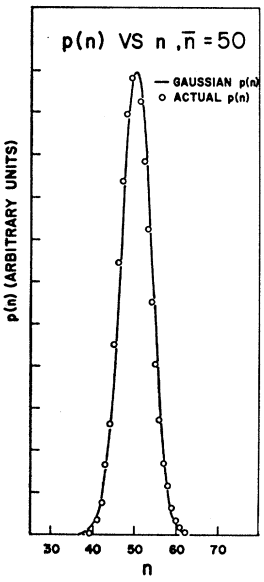

FIG. 13. Gaussian probability distribution, Eq. (17), compared with Eq. (16). The departures of the actual distribution from the Gaussian distribution are not experimentally distinguishable.

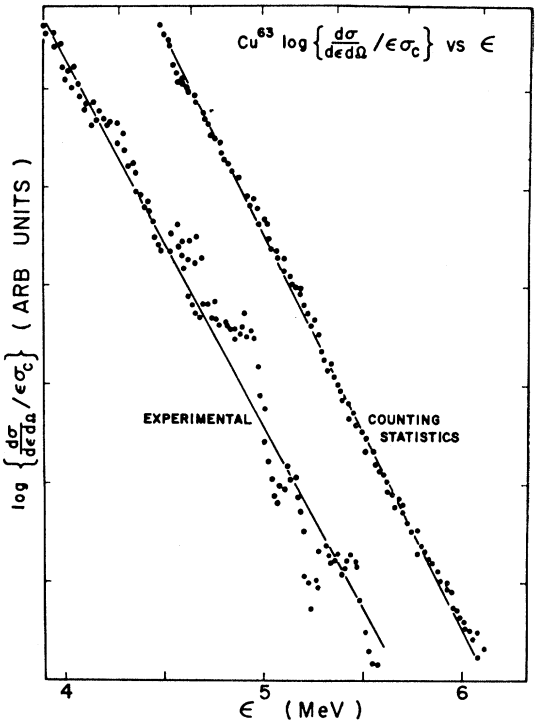

FIG. 14. Comparison of experimental data with simulated data composed of average values plus counting statistics effects. The counting statistics curve is displaced to the right.

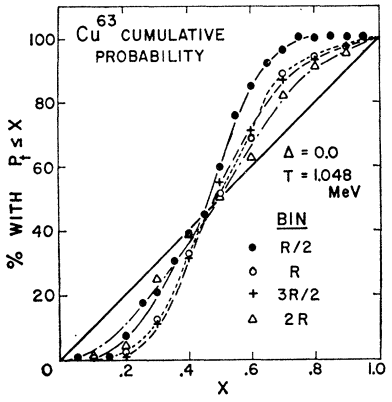

FIG. 15. Cu^{63} cumulative probability plot, percentage of bins with $P_t \leq x$ versus x, for bins with widths varying from half the resolution width to twice the resolution width.

than the bin width B. Figure 15 shows the results of varying B from $R/2$ to $2R$ with $K=0.27$ for Cu^{63} with $T=1.048$ and $\Delta=0$, over an excitation region ranging from 3.0 to 7.0 MeV. The resolution dependence is roughly what is expected. When the binwidth is too small, the observed distribution is narrower than the assumed gaussian of variance 0.27 $(\bar{\eta}-1)$ due to the smoothing effect of yields spilling into adjacent bins. As B is increased, the variance approaches the Wigner value. Figure 15 indicated that bin sizes of $B=2R$ are large enough to avoid smoothing of the η fluctuations due to energy resolution effects. Picking the largest practical bin sizes, $B=2R$, cumulative probability P_t, curves were drawn for Cu^{63}, Zn^{66}, and Zn^{64} using $0.1 \leq K \leq 0.3$. The departures from a straight line in Fig. 16 demonstrate that the η fluctuations may be described by a gaussian distribution with $\mathrm{Var}(\bar{\eta})=\sigma^2 = K(\bar{\eta}-1)$, where $0.1 \leq K \leq 0.3$ for the nuclei studied in this experiment.

In the above analysis of yield fluctuations we have taken the parameters T from the evaporation spectra and Δ from the (p,p') to (p,α) yield ratios. The fluctuations were then used to obtain the variance of the level number distribution. In principle, the procedure could be inverted if the form of the number distribution were known. The temperature would again be taken from spectra and the fluctuations then used to determine the gap parameter, Δ. This procedure will be illustrated by determining Δ from high resolution direct level count data in Sec. V.

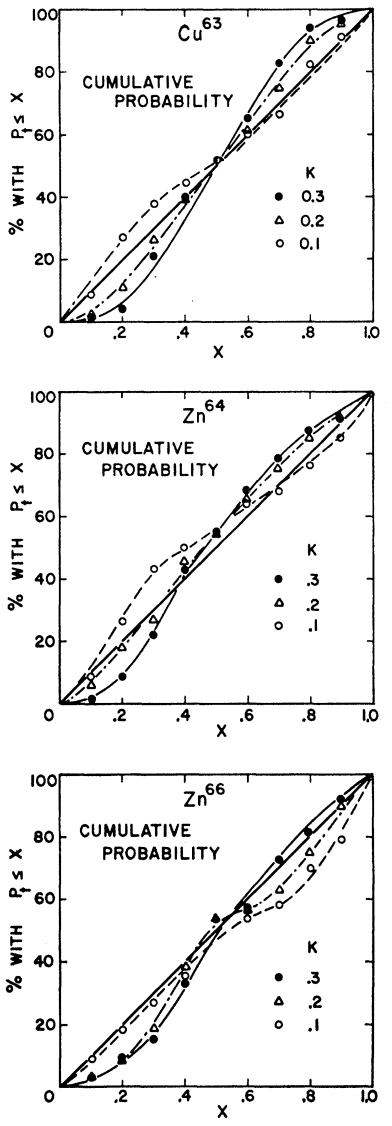

FIG. 16. Cumulative probability plots for Cu^{63}, Zn^{64}, and Zn^{66}. $B=2R$ and $0 \leq x \leq 1$. The solid line is the curve expected if the experimental distribution has $\mathrm{Var}(N)=K\bar{N}$. The Δ's for the even-even nuclei are yield-ratio values given in Table IX.

V. DIRECT-LEVEL-COUNT FLUCTUATIONS

As a test of the methods used in analyzing fluctuations in our continuous inelastic spectra, we have taken data

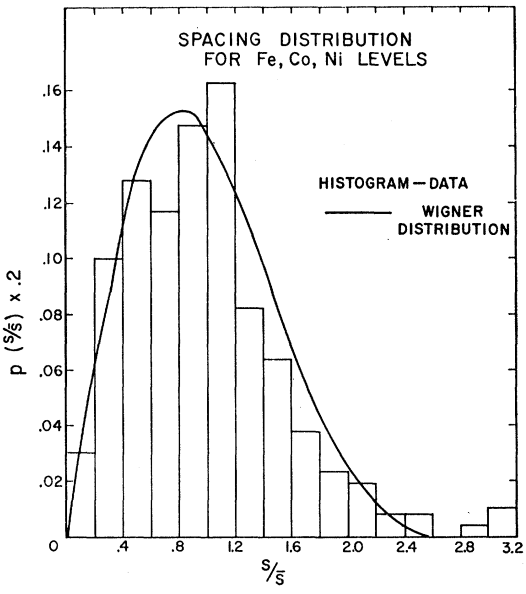

FIG. 17. Spacing distribution for 265 spacings for Fe^{56}, Co^{59}, Ni^{59}, and Ni^{61} levels below ~6 MeV, plotted against ratio of spacing to average spacing. The smooth curve shows a Wigner distribution for levels of a single J, π.

TABLE XI. Comparison of T's and Δ's for high-resolution level-count data (Refs. 34 and 35) obtained by various methods.

Nucleus	P_t plots T (MeV)	P_t plots Δ (MeV)	Best fit by eye T (MeV)	Best fit by eye Δ (MeV)	Gilbert *et al.* analysis[a] T (MeV)	Gilbert *et al.* analysis[a] Δ (MeV)
Ni^{59}	1.20±0.02	−0.64 ±0.02	1.20 ±0.05	−0.64 ±0.2	1.51	−1.75
Ni^{61}	1.38±0.01	−1.42 ±0.04	1.38 ±0.03	−1.60 ±0.1	1.29	−1.25
Cu^{63}	0.97±0.01	−0.32 ±0.02	0.914±0.04	0 ±0.2	0.98	−0.25
Fe^{56}	1.44±0.01	−0.075±0.01	1.44 ±0.02	−0.080±0.12	1.26	0.60
Co^{59}	0.98±0.01	−0.077±0.01	0.98 ±0.02	−0.31 ±0.12	1.06	−0.40

[a] Reference 30.

from high-resolution experiments[34,35] in which individual states were resolved to examine the nearest-neighbor level-spacing distribution as well as the level numbers distribution.

The nearest-neighbor level-spacing distribution was obtained for 265 level spacings in Ni^{59}, Ni^{61}, Co^{59}, and Fe^{56}. A $N(U)$ plot was constructed for each of these nuclei and $N(U)$ was read from the graph for each spacing to give the average spacing at that excitation using $\bar{s}=T/\bar{N}$. Figure 17 shows the resultant spacing histogram plotted against the ratio of the spacing to the average spacing, $\bar{s}$. This histogram appears to follow a Wigner distribution more closely than an exponential distribution and indicates that level spacings at excitations up to ~6 MeV for these nuclei still exhibit sufficient regularity to retain some of the Wigner shape characteristic of levels of a single J, π. Katsanos *et al.*[35] have studied 55 Fe^{54-58} and Fe^{59} level spacings and found agreement with the exponential spacing distribution corresponding to a random-spacing distribution. However, in their analysis, the average spacing $\bar{s}$ was assumed constant over a 1 MeV interval in which the actual $\bar{s}$ varied by a factor of ~2. Thus many spacings were found which were smaller than their assumed $\bar{s}$.

P_t plots were made in Sec. IV from the spectrum data by choosing nonoverlapping bins of constant width. This procedure is impractical for the high-resolution level-count data so a different method was used. All bins were chosen with a common lower edge at the fourth or fifth excited state. Successive bins were chosen to include one additional level in each new bin. The average number of levels in each bin was found from $N(U)$ T's and Δ's. Level numbers ranged from 4 for the narrowest to 100 for the widest bins.

T and Δ were then varied from initial values to get the best CP_t plots. Figures 18 and 19 show, when the requirement is imposed that the fraction of bins with $CP_t \leq 0.5$ equals 0.5 (necessary for $\bar{\eta}_{\text{exp}}=\bar{\eta}_{\text{theo}}$), a small range of permissible T and Δ is defined. Table XI lists the T's and Δ's found by imposing this requirement on the P_t plots. The values of T and Δ are somewhat different from those of Gilbert *et al.*,[30] who used somewhat earlier data.

After finding the best values of T and Δ, as described above, K was varied over the range $0.1 \leq K \leq 0.3$. Figure 20 shows that the resulting CP_t plots indicate $K \simeq 0.2$ for Fe^{56}, Co^{59}, and Cu^{63}.

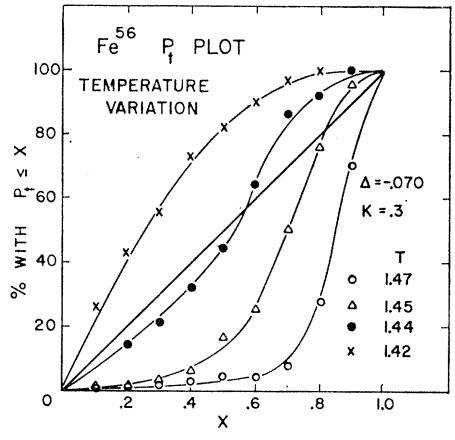

FIG. 18. Cumulative probability plot for Fe^{56} level-count data, Δ and K fixed, varying T.

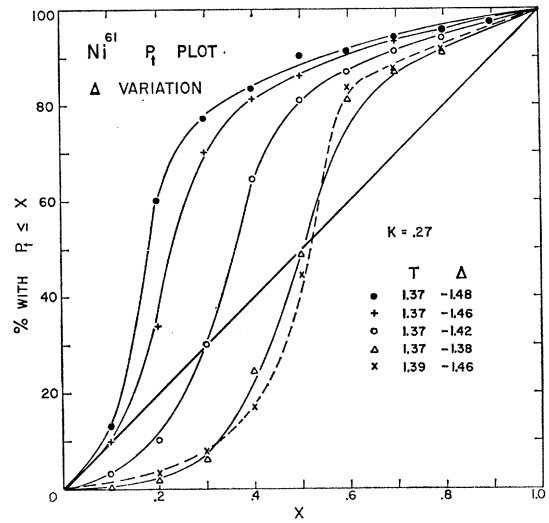

FIG. 19. Cumulative probability plot for Ni^{61} level-count data, K and T fixed (except for last Δ), varying Δ.

[34] ONR Generator Group, Massachusetts Institute of Technology Nuclear Science Laboratory Progress Report No. 109, 1959 (unpublished).

[35] A. A. Katsanos, J. R. Huizenga, and H. K. Vonach, Phys. Rev. 141, 1053 (1966).

VI. SUMMARY AND CONCLUSIONS

The angular distributions for (p,p') and (p,α) yields to moderate excitation regions ($U\sim 2$–7 MeV) of the residual nuclei Cu^{63}, Cu^{65}, Zn^{66}, and Ni^{58} were found to be symmetric about 90° and nearly isotropic. When the excitation region of the residual nucleus included lower excitation regions, the anisotropy increased slightly indicating a decrease in the spin cutoff parameter σ. Inelastic proton yield curves for Cu^{63} and Zn^{66} indicated some possible intermediate or doorway state resonance structure. Nuclear temperatures from alpha and proton spectra were found to agree to within $\pm 10\%$ with temperatures from $N(U)$ plots when the temperatures were determined over nearby excitation regions. The temperatures, however, showed a slow increase with bombarding energy, even when T was calculated from residual nuclear excitation regions $\gtrsim 3$ MeV. This effect is perhaps due to the neglect of angular momentum in the compound statistical theory used or to small direct interaction contributions. The energy gaps Δ calculated from proton-to-alpha-yield ratios, agreed with Δ's determined from the $N(U)$ plots to within their errors, and with Δ from pairing energies calculated by Cameron to within $\pm 7\%$. Departures from the average inelastic yields in neighboring energy bins were found to be understandable in terms of fluctuations in the number of levels per bin, η, where $\mathrm{Var}(\eta)=K(\bar{\eta}-1)$. K was found to range from about 0.3 to 0.1. A value $K=0.27$ is expected for a Wigner distributiou. High-resolution level-count data were used to obtain spacing- and level-numbers distributions. Cumulative probability plots were used to find T and Δ for Fe^{56}, Co^{59}, Ni^{59}, Ni^{61}, and Cu^{63}. These elements showed a numbers distribution with a variance of approximately $0.2(\bar{\eta}-1)$.

The consistency of nuclear evaporation temperatures with $N(U)$ plots, the linearity of temperature plots from spectra (evidenced by the standard error in T), the consistency of the various Δ's, the departures in $\bar{\eta}$ from their average values (roughly consistent with those expected for a Wigner distribution), all indicate the adequacy of the simple form, $(1/T)e^{(U-\Delta)/T}$, for the nuclear level density over the excitation range covered by the experiment. Further, the results support the fundamental assumptions of the compound statistical model since the yield fluctuations between neighboring energy intervals are consistent with fluctuations in the level number in those intervals.

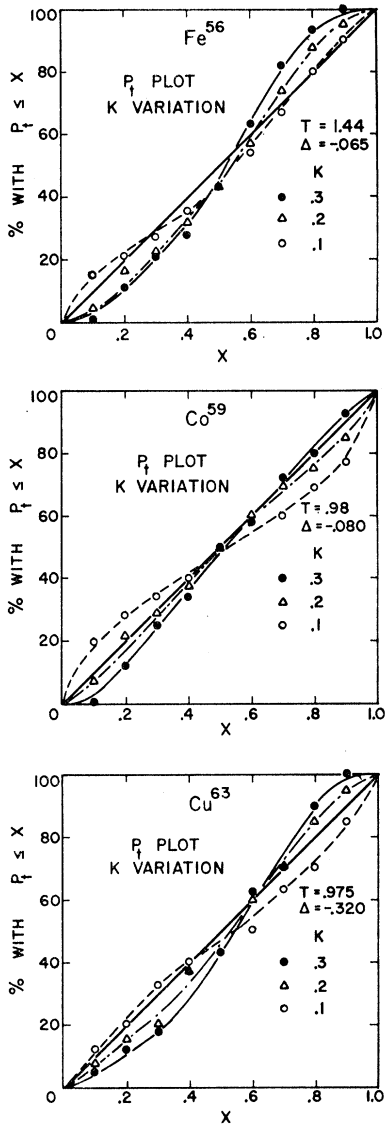

FIG. 20. Cumulative probability plots for Fe^{56}, Co^{59}, Cu^{63}, T, and Δ fixed, varying K. Best value seems to be $K\simeq 0.2$.

ACKNOWLEDGMENTS

The authors wish to thank the technical staff of the University of Minnesota linear accelerator and of the Argonne tandem. We are indebted to Dr. F. W. Briese for his lucid descriptions of mathematical statistics.